Seismic metasurfaces on porous layered media: Surface resonators and fluid-solid interaction effects on the propagation of Rayleigh waves

Published in International Journal of Engineering Science (2020)
doi.org/10.1016/j.ijengsci.2020.103347

Seismic metasurfaces on porous layered media: surface resonators and fluid-solid interaction effects on the propagation of Rayleigh waves

Xingbo Pu[a,1], Antonio Palermo[a,1], Zhibao Cheng[b], Zhifei Shi[b], Alessandro Marzani[a,*]

[a]*Department of Civil, Chemical, Environmental and Materials Engineering - DICAM, University of Bologna, 40136 Bologna, Italy*

[b]*Institute of Smart Materials and Structures, School of Civil Engineering, Beijing Jiaotong University, Beijing, 100044, China*

Abstract

Seismic surface wave mitigation using metamaterials is a growing research field propelled by intrinsic theoretical value and possible application prospects. Up to date, the complexity of site conditions found in engineering practice, which can include layered stratigraphy and variable water table level, has been discarded in the development of analytical frameworks to favor the derivation of simple, yet effective, closed-form dispersion laws. This work provides a further step towards the analytical study of "seismic metasurfaces" in real site conditions considering the propagation of Rayleigh waves through a layered porous substrate equipped with local resonators. To this aim, we combine classical elasticity theory, Biot's poroelasticity and an effective medium approach to describe the metasurface dynamics and its coupling with the poroelastic substrate. The developed framework naturally includes simpler configurations like seismic metasurfaces atop homogeneous dry or saturated soils. Apart from known phenomena like wave-resonance hybridization and surface wave band gaps, we predict the existence of an extended frequency range where surface waves are attenuated due to energy leakage in the form of slow pressure waves, as a result of the fluid-solid interaction. Besides, we demonstrate that the surface wave band-gap and the related surface-to-shear wave conversion is robust to variations in the water table level. Conversely, when the dry and saturated layers have different material parameters, for example, due to different porosity ratios, the surface-to-shear wave conversion can be accompanied by the excitation of higher-order surface modes, which remain channeled below the metasurface. These analytical findings, augmented and confirmed by numerical simulations, evidence the importance of accounting for fluid-solid interaction in the dynamics of seismic metasurfaces.

Keywords: Metamaterials, Rayleigh waves, Biot's theory, fluid-solid interaction, band gaps

1. Introduction

In the last couple of decades, studies on artificial media endowed with a periodic structure or local resonant elements, also known as metamaterials, have fostered the development of novel devices for electromagnetic, acoustic and elastic waves control across different length and frequency scales [1, 2, 3]. Despite their difference in size and target frequency, all metamaterials exploit a purposely designed internal architecture to manipulate the dispersive properties of waves and achieve unique dynamic features, like frequency band gaps [4, 5], enhanced waveguiding abilities [6, 7] and high energy absorption [8, 9].

When low-frequency elastic waves are of interest, as in the context of civil engineering, the use of locally resonant materials can be particularly appealing since they allow the mitigation of vibrations with compact, i.e., sub-wavelength, structures. Following this idea, meter-size resonant devices either integrated into the building foundations [10, 11, 12, 13], or buried around target structures [14, 15, 16], have been recently proposed as an alternative solution for ground-borne vibration reduction and seismic isolation. When the resonators are arranged along the soil surface, to form a "metabarrier" [16] or "seismic metasurface" [17], they can be designed to impede the propagation of surface waves. In particular, the mitigation of vertically polarized surface waves, i.e., Rayleigh-like waves, is of primary interest since they carry the most significant portion of the elastic energy which propagates along the surface. The ability of mitigating their amplitude stems from the hybridization between the surface motion and the resonator localized modes, which results in the generation of surface wave band gaps around the resonator natural frequencies [18, 19]. The hybridization can also be exploited to tune phase velocities and the wavelengths of propagating waves thus offering further possibilities for surface wave

*Corresponding author
Email address: alessandro.marzani@unibo.it (Alessandro Marzani)
[1]The authors contribute equally to the work.

control. These unique features have been predicted and observed in natural and artificial metasurfaces, such as forest of trees [20, 21], rows of piles [22], resonant wave barriers [16] and "metawedges" [23].

Notwithstanding their pioneering contributions, which have greatly promoted the development of seismic metasurfaces, existing researches have considered the metasurface substrate as a single-phase homogeneous elastic medium, a simplistic model which is not always sufficient to capture the complexity of soils. Indeed, soils are typically characterized by a horizontal stratification accompanied by the presence of fluids, generally water, which can saturate some of the layers. As both the stratigraphy and the presence of water in the soil modify the propagation of bulk and surface waves, it is of interest to investigate the metasurface behavior in such a context.

This work, in particular, aims at unveiling the dynamics of a metasurface coupled to a half-space which is fully saturated up to a certain depth, thus modeling the presence of different water table levels. To this purpose, the soil beneath the metasurface is modeled as a dry porous layer coupled to a fully saturated half-space. While the dry elastic layer supports a pressure (P) and a shear (S) bulk wave, according to the Biot's theory, the saturated porous medium supports three types of bulk waves: two pressure waves and a shear wave [24, 25]. The fast pressure wave (P1 wave) and the shear wave are almost analogous to the P and S waves of the dry medium, while the slow pressure wave (P2 wave) is associated with a diffusion-type process [26]. Hence, in contrast to a single-phase elastic half-space, the dynamics of surface waves propagating in such a porous layered system involves the interaction of multiple body waves. This interaction is expected to provide peculiar features to the dynamics of metasurfaces which is today not yet described. Therefore, the purpose of this work is to develop a theoretical framework to discuss the dynamics of a seismic metasurface composed of resonators placed on a porous medium and considering part of it fully saturated. In particular, our main interest is focused on the determination of the dispersive properties of Rayleigh-like waves, including band gaps, mode-conversion phenomena and wave attenuation, and their dependence on some porous medium fundamental parameters like tortuosity, viscosity and water table.

The paper is organized as follows. Without loss of generality, we model the metasurface as an array of vertical mass-spring resonators attached to a porous half-space with a given water table level and derive the dispersion equation of Rayleigh-like waves in Section 2. This derivation naturally allows the description of two simpler configurations: the metasurface on homogeneous dry and saturated half-spaces, respectively. The derived analytical dispersion equation is validated via comparisons with Finite Element (FE) solutions in Section 3. In Section 4, we discuss the effect of tortuosity, viscosity and water table level on dispersion curves. We also adopt the FE model to validate the novel phenomena predicted by the dispersion equation. Finally, some concluding remarks are provided in Section 5.

2. Analytical framework

This section aims at deriving the surface-wave dispersion equation for a metasurface laying on a porous medium with a given water table level. To this end, we restrict our investigation to a plane-strain problem, considering a bi-layer system, i.e., a dry soil layer over a fully saturated half-space. Next, we prove that the obtained dispersion relation reduces to those of two simpler configurations (i) a dry porous half-space and (ii) a fully saturated half-space, when the water table level is at infinite depth or at the soil surface, respectively. We remark that our interest is on low-frequency waves, as per the seismic context, and thus the metasurface can be modeled through an effective medium approach and the saturated soil via classical homogenized theories, as the wavelengths involved are larger than the resonator dimensions and soil heterogeneity, respectively.

2.1. A metasurface over a porous half-space with generic water table level

The configuration of interest is shown in Fig. 1, which schematically represents a porous half-space coupled with a metasurface. The upper part of the half-space is a dry layer of thickness h, in which the wave propagation can be properly described by the classical elasticity theory [25, 27]. Conversely, for $z > h$ the porous medium is fully saturated due to the presence of water (see the representative volume element (RVE) shown in the inset of Fig. 1). Within this medium, fluid-solid interaction phenomena arise, which can be treated via Biot's theory [28, 29] assuming an RVE characteristic length much smaller than the wavelength of interest, as per our focus on low-frequency seismic wave propagation. For the metasurface, we consider the canonical configuration composed of mass-spring resonators, arranged in an array with lattice distance D [19, 30]. For the porous substrate, we consider the generic configuration of a dry layer with mechanical parameters possibly different from the ones of the skeleton of the saturated half-space. Indeed, our analysis will mainly focus on the simpler scenario where the dry layer and the skeleton of the saturated half-space have the same mechanical properties. In what follows we detail the theoretical derivation to obtain the metasurface dispersion relation.

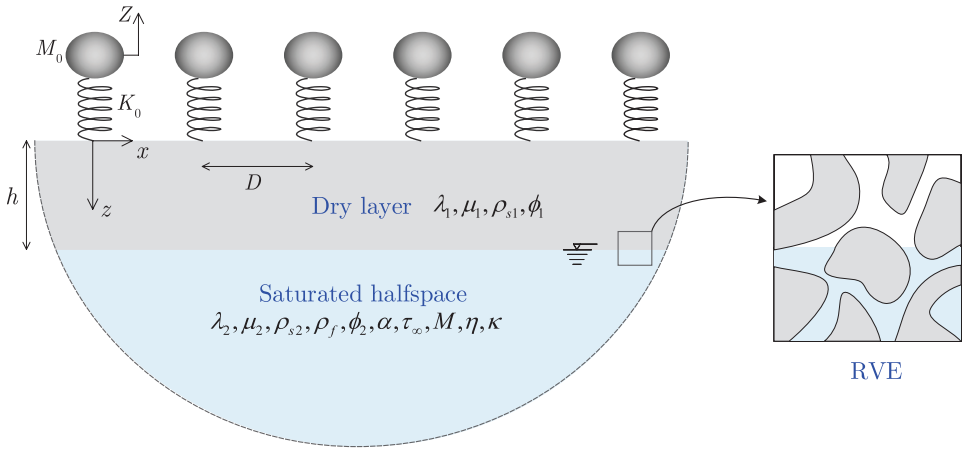

Fig. 1. Schematic of a seismic metasurface on a porous layered medium.

2.1.1. Wave motion in the dry layer

In the absence of body forces, the governing equation of motion in the dry porous layer can be written as:

$$(\lambda_1+\mu_1)\nabla(\nabla\cdot\boldsymbol{u})+\mu_1\nabla^2\boldsymbol{u}=\rho_d\frac{\partial^2\boldsymbol{u}}{\partial t^2}, \tag{1}$$

in which λ_1,μ_1 are the skeleton Lamé constants, $\boldsymbol{u}=[u_x,u_z]$ is the displacement vector, $\nabla=(\partial/\partial x,\partial/\partial z)$ is the gradient operator, and $\rho_d=(1-\phi_1)\rho_{s1}$ is the dry mass density, where ϕ_1 is the porosity and ρ_{s1} is the density of the grains. The components of the displacement vector, according to the Helmholtz decomposition $\boldsymbol{u}=\nabla\Phi+\nabla\times\boldsymbol{\Psi}$, can be expressed as:

$$u_x=\frac{\partial\Phi}{\partial x}-\frac{\partial\Psi_y}{\partial z},\quad u_z=\frac{\partial\Phi}{\partial z}+\frac{\partial\Psi_y}{\partial x} \tag{2}$$

in which Φ is a scalar potential and Ψ_y is a component of the vector potential $\boldsymbol{\Psi}$. Substituting Eq. (2) into Eq. (1) yields two uncoupled equations:

$$\nabla^2\Phi=\frac{1}{C_P^2}\frac{\partial^2\Phi}{\partial t^2},\quad \nabla^2\Psi_y=\frac{1}{C_S^2}\frac{\partial^2\Psi_y}{\partial t^2} \tag{3}$$

in which C_P and C_S represent the velocity of pressure and shear waves in the dry soil, namely:

$$C_P=\sqrt{\frac{\lambda_1+2\mu_1}{\rho_d}},\quad C_S=\sqrt{\frac{\mu_1}{\rho_d}} \tag{4}$$

Assuming harmonic waves propagating along the x direction with angular frequency ω and wave number k, the potential functions can be chosen as:

$$\Phi=\left(A_1e^{-pz}+B_1e^{pz}\right)e^{i(\omega t-kx)}, \tag{5a}$$

$$\Psi_y=\left(A_2e^{-qz}+B_2e^{qz}\right)e^{i(\omega t-kx)} \tag{5b}$$

where A_1, A_2, B_1, B_2 are the amplitudes of the potentials, and the wave numbers components along the z-axis are expressed as:

$$p=\sqrt{k^2-\frac{\omega^2}{C_P^2}},\quad q=\sqrt{k^2-\frac{\omega^2}{C_S^2}}. \tag{6}$$

Substituting Eq. (5) into Eq. (2) yields the displacement components as:

$$u_x=\left[-ik\left(A_1e^{-pz}+B_1e^{pz}\right)+q\left(A_2e^{-qz}-B_2e^{qz}\right)\right]e^{i(\omega t-kx)} \tag{7a}$$

$$u_z=\left[-p\left(A_1e^{-pz}-B_1e^{pz}\right)-ik\left(A_2e^{-qz}+B_2e^{qz}\right)\right]e^{i(\omega t-kx)} \tag{7b}$$

from which the stress components, according to Hooke's law, can be derived as follows:

$$\begin{aligned}\sigma_{zz} &= \lambda_1 \frac{\partial u_x}{\partial x} + (\lambda_1 + 2\mu_1)\frac{\partial u_z}{\partial z} \\ &= \mu_1 \left[\left(k^2 + q^2\right)\left(A_1 e^{-pz} + B_1 e^{pz}\right) + 2ikq\left(A_2 e^{-qz} - B_2 e^{qz}\right)\right] e^{i(\omega t - kx)}\end{aligned} \tag{8a}$$

$$\begin{aligned}\tau_{zx} &= \mu_1 \left(\frac{\partial u_x}{\partial z} + \frac{\partial u_z}{\partial x}\right) \\ &= \mu_1 \left[2ikp\left(A_1 e^{-pz} - B_1 e^{pz}\right) - \left(k^2 + q^2\right)\left(A_2 e^{-qz} + B_2 e^{qz}\right)\right] e^{i(\omega t - kx)}\end{aligned} \tag{8b}$$

2.1.2. Wave motion in the saturated half-space

Bulk waves in a saturated medium. Following Biot's theory [28, 29], the governing equations for wave motion in the saturated soil can be expressed according to the $\boldsymbol{u} - \boldsymbol{w}$ formulation, where $\boldsymbol{u}$ is the displacement vector of the solid skeleton and $\boldsymbol{w}$ is the relative displacement of the fluid to the solid skeleton, as:

$$(\lambda_2 + \mu_2 + \alpha^2 M)\nabla(\nabla \cdot \boldsymbol{u}) + \mu_2 \nabla^2 \boldsymbol{u} + \alpha M \nabla(\nabla \cdot \boldsymbol{w}) = \rho \frac{\partial^2 \boldsymbol{u}}{\partial t^2} + \rho_f \frac{\partial^2 \boldsymbol{w}}{\partial t^2} \tag{9a}$$

$$\alpha M \nabla(\nabla \cdot \boldsymbol{u}) + M \nabla(\nabla \cdot \boldsymbol{w}) = \rho_f \frac{\partial^2 \boldsymbol{u}}{\partial t^2} + m \frac{\partial^2 \boldsymbol{w}}{\partial t^2} + b \frac{\partial \boldsymbol{w}}{\partial t} \tag{9b}$$

where λ_2 and μ_2 are the Lamé constants of the skeleton, ρ_f is the fluid mass density, and ρ is the total mass density expressed as $\rho = \phi_2 \rho_f + (1 - \phi_2)\rho_{s2}$, where ϕ_2 and ρ_{s2} are the porosity and grain density of the half-space. The parameter $m = \tau_\infty \rho_f / \phi_2$ describes the relation between the fluid density and the geometry of the pores, where τ_∞ is the tortuosity, usually determined via experiments [27]. The parameter $b = \eta/\kappa$ describes the viscous coupling between the solid and the fluid, with η being the fluid viscosity and κ the permeability. The parameters α and M account for the compressibility and coupling modulus, respectively:

$$\alpha = 1 - \frac{K_d}{K_s}; \quad \frac{1}{M} = \left(\frac{\alpha - \phi_2}{K_s} + \frac{\phi_2}{K_f}\right) \tag{10}$$

where K_d is the drained bulk modulus of the solid skeleton and is given by $K_d = \lambda_2 + 2\mu_2/3$, K_s is the bulk modulus of solid grains and K_f is the bulk modulus of the fluid phase. Typically, the parameter α is bounded by $\phi_2 \leq \alpha \leq 1$ and $0 \leq M < +\infty$ [25].

Similarly to the procedure followed for the dry layer, we consider a Helmholtz decomposition of the displacement fields as:

$$\boldsymbol{u} = \nabla \Phi_s + \nabla \times \boldsymbol{\Psi}_s, \quad \boldsymbol{w} = \nabla \Phi_f + \nabla \times \boldsymbol{\Psi}_f \tag{11}$$

where Φ_s and $\boldsymbol{\Psi}_s$ represent the scalar potential and the vector potential of the solid, respectively, while Φ_f and $\boldsymbol{\Psi}_f$ are the potentials associated with the fluid motion relative to the solid. A substitution of Eq. (11) into Eq. (9) allows to obtain the uncoupled governing equations of motion for P waves:

$$(\lambda_2 + 2\mu_2 + \alpha^2 M)\nabla^2 \Phi_s + \alpha M \nabla^2 \Phi_f = \rho \frac{\partial^2 \Phi_s}{\partial t^2} + \rho_f \frac{\partial^2 \Phi_f}{\partial t^2} \tag{12a}$$

$$\alpha M \nabla^2 \Phi_s + M \nabla^2 \Phi_f = \rho_f \frac{\partial^2 \Phi_s}{\partial t^2} + m \frac{\partial^2 \Phi_f}{\partial t^2} + b \frac{\partial \Phi_f}{\partial t} \tag{12b}$$

and for S waves:

$$\mu_2 \nabla^2 \boldsymbol{\Psi}_s = \rho \frac{\partial^2 \boldsymbol{\Psi}_s}{\partial t^2} + \rho_f \frac{\partial^2 \boldsymbol{\Psi}_f}{\partial t^2} \tag{13a}$$

$$\rho_f \frac{\partial^2 \boldsymbol{\Psi}_s}{\partial t^2} + m \frac{\partial^2 \boldsymbol{\Psi}_f}{\partial t^2} + b \frac{\partial \boldsymbol{\Psi}_f}{\partial t} = 0 \tag{13b}$$

We consider the general solutions of Eqs. (12) and (13) in the following form [26]:

$$[\Phi_s, \Phi_f]^T = [A_s, A_f]^T e^{i(\omega t - \boldsymbol{k}_P \cdot \boldsymbol{r})} \tag{14a}$$

$$[\Psi_{sy}, \Psi_{fy}]^T = [B_s, B_f]^T e^{i(\omega t - \boldsymbol{k}_S \cdot \boldsymbol{r})} \tag{14b}$$

where Ψ_{sy} and Ψ_{fy} are the components of the vector potential $\boldsymbol{\Psi}$, $\boldsymbol{k}_P$ and $\boldsymbol{k}_S$ are wave vectors of P wave and S wave, respectively, and $\boldsymbol{r}$ is the position vector. Substituting Eq. (14a) into Eq. (12) yields the characteristic

equation for P waves:

$$\begin{bmatrix} \rho\omega^2 - \left(\lambda_2 + 2\mu_2 + \alpha^2 M\right) k_P^2 & \rho_f\omega^2 - \alpha M k_P^2 \\ \rho_f\omega^2 - \alpha M k_P^2 & \rho_c\omega^2 - M k_P^2 \end{bmatrix} \begin{bmatrix} A_s \\ A_f \end{bmatrix} = \mathbf{0} \tag{15}$$

where $\rho_c = m - ib/\omega$. Eq. (15) has two nontrivial solutions:

$$c_{P1}^2 = \frac{\omega^2}{k_{P1}^2} = \frac{R_1 + \sqrt{R_1^2 - 4R_2}}{2R_2}, \quad c_{P2}^2 = \frac{\omega^2}{k_{P2}^2} = \frac{R_1 - \sqrt{R_1^2 - 4R_2}}{2R_2} \tag{16}$$

where c_{P1} and c_{P2} denote the velocities of P1 and P2 bulk waves in the saturated soil, respectively, whereas the coefficients R_1 and R_2 are expressed as:

$$R_1 = \frac{(\lambda_2 + 2\mu_2 + \alpha^2 M)\rho_c - 2\alpha M \rho_f + M\rho}{(\lambda_2 + 2\mu_2)M}, \quad R_2 = \frac{\rho\rho_c - \rho_f^2}{(\lambda_2 + 2\mu_2)M} \tag{17}$$

Similarly, substituting Eq. (14b) into Eq. (13) yields the characteristic equation for the S waves:

$$\begin{bmatrix} \rho\omega^2 - \mu_2 k_S^2 & \rho_f\omega^2 \\ \rho_f\omega^2 & \rho_c\omega^2 \end{bmatrix} \begin{bmatrix} B_s \\ B_f \end{bmatrix} = \mathbf{0} \tag{18}$$

which has one nontrivial solution:

$$c_S^2 = \frac{\omega^2}{k_S^2} = \frac{\mu_2}{(\rho - \rho_f^2/\rho_c)} \tag{19}$$

where c_S represents the shear wave velocity in a saturated soil.

Surface waves in a saturated half-space. Given the bulk velocities in the fluid saturated medium (Eqs. (16, 19)), we can proceed in looking for surface wave solutions. For harmonic surface waves traveling in the x direction and decaying exponentially in the z direction, the four potential functions in the saturated half-space can be expressed as [31]:

$$\Phi_s = \left(\bar{A}_1 e^{-Q_1 z} + \bar{A}_2 e^{-Q_2 z}\right) e^{i(\omega t - kx)} \tag{20a}$$

$$\Phi_f = \left(\bar{A}_1 \delta_1 e^{-Q_1 z} + \bar{A}_2 \delta_2 e^{-Q_2 z}\right) e^{i(\omega t - kx)} \tag{20b}$$

$$\Psi_{sy} = \bar{A}_3 e^{-Q_3 z} e^{i(\omega t - kx)} \tag{20c}$$

$$\Psi_{fy} = \bar{A}_3 \delta_3 e^{-Q_3 z} e^{i(\omega t - kx)} \tag{20d}$$

where $\bar{A}_j$ $(j = 1, 2, 3)$ are the corresponding amplitudes, δ_i $(i = 1, 2, 3)$ are the ratios of the potential functions amplitudes as:

$$\delta_1 = \frac{A_{f1}}{A_{s1}} = \frac{\rho_f c_{P1}^2 - \alpha M}{M - \rho_c c_{P1}^2} \tag{21a}$$

$$\delta_2 = \frac{A_{f2}}{A_{s2}} = \frac{\rho_f c_{P2}^2 - \alpha M}{M - \rho_c c_{P2}^2} \tag{21b}$$

$$\delta_3 = \frac{B_f}{B_s} = -\frac{\rho_f}{\rho_c} \tag{21c}$$

and the wave numbers are expressed as:

$$Q_1 = \sqrt{k^2 - k_{P1}^2}, \quad Q_2 = \sqrt{k^2 - k_{P2}^2}, \quad Q_3 = \sqrt{k^2 - k_S^2} \tag{22}$$

By substituting Eq. (20) into Eq. (11), the displacements in the skeleton are expressed as:

$$u_x = \frac{\partial \Phi_s}{\partial x} - \frac{\partial \Psi_{sy}}{\partial z} = \left[-ik\left(\bar{A}_1 e^{-Q_1 z} + \bar{A}_2 e^{-Q_2 z}\right) + \bar{A}_3 Q_3 e^{-Q_3 z}\right] e^{i(\omega t - kx)} \tag{23a}$$

$$u_z = \frac{\partial \Phi_s}{\partial z} + \frac{\partial \Psi_{sy}}{\partial x} = \left(-\bar{A}_1 Q_1 e^{-Q_1 z} - \bar{A}_2 Q_2 e^{-Q_2 z} - ik\bar{A}_3 e^{-Q_3 z}\right) e^{i(\omega t - kx)} \tag{23b}$$

whereas the relative displacements in the fluid are:

$$w_x = \frac{\partial \Phi_f}{\partial x} - \frac{\partial \Psi_{fy}}{\partial z} = \left[-ik\left(\bar{A}_1\delta_1 e^{-Q_1 z} + \bar{A}_2\delta_2 e^{-Q_2 z}\right) + \bar{A}_3\delta_3 Q_3 e^{-Q_3 z}\right] e^{i(\omega t - kx)} \tag{24a}$$

$$w_z = \frac{\partial \Phi_f}{\partial z} + \frac{\partial \Psi_{fy}}{\partial x} = \left(-\bar{A}_1\delta_1 Q_1 e^{-Q_1 z} - \bar{A}_2\delta_2 Q_2 e^{-Q_2 z} - ik\bar{A}_3\delta_3 e^{-Q_3 z}\right) e^{i(\omega t - kx)} \tag{24b}$$

Assuming isotropic linear elastic constitutive relationships, the total stresses and the pore pressure can be written as:

$$\begin{aligned}\sigma_{zz} &= \lambda_2 \frac{\partial u_x}{\partial x} + (\lambda_2 + 2\mu_2)\frac{\partial u_z}{\partial z} - \alpha p_f \\ &= \left[-\left(\lambda_2 + \alpha^2 M + \alpha M \delta_1\right) k_{P1}^2 + 2\mu_2 Q_1^2\right] \bar{A}_1 e^{-Q_1 z} e^{i(\omega t - kx)} \\ &+ \left[-\left(\lambda_2 + \alpha^2 M + \alpha M \delta_2\right) k_{P2}^2 + 2\mu_2 Q_2^2\right] \bar{A}_2 e^{-Q_2 z} e^{i(\omega t - kx)} \\ &+ 2i\mu_2 k Q_3 \bar{A}_3 e^{-Q_3 z} e^{i(\omega t - kx)}\end{aligned} \tag{25a}$$

$$\begin{aligned}\tau_{zx} &= \mu_2\left(\frac{\partial u_x}{\partial z} + \frac{\partial u_z}{\partial x}\right) \\ &= \mu_2\left[2ikQ_1\bar{A}_1 e^{-Q_1 z} + 2ikQ_2\bar{A}_2 e^{-Q_2 z} - (2k^2 - k_S^2)\bar{A}_3 e^{-Q_3 z}\right] e^{i(\omega t - kx)}\end{aligned} \tag{25b}$$

$$\begin{aligned}p_f &= -M\left(\frac{\partial w_x}{\partial x} + \frac{\partial w_z}{\partial z}\right) - \alpha M\left(\frac{\partial u_x}{\partial x} + \frac{\partial u_z}{\partial z}\right) \\ &= \left[M(\alpha + \delta_1)k_{P1}^2 \bar{A}_1 e^{-Q_1 z} + M(\alpha + \delta_2)k_{P2}^2 \bar{A}_2 e^{-Q_2 z}\right] e^{i(\omega t - kx)}\end{aligned} \tag{25c}$$

2.1.3. Dynamics of the resonator

As last element of our analytical derivation, we consider the governing equation of a mass-spring resonator coupled to the free surface ($z = 0$) of the soil:

$$M_0 \frac{d^2 Z}{dt^2} + K_0 (Z + u_z) = 0 \tag{26}$$

where M_0 is the resonator mass, K_0 is the spring stiffness, Z is the vertical displacement of the resonator, and u_z is the vertical displacement at the contact point of the resonator with the free surface. Assuming a harmonic form $e^{i(\omega t - kx)}$ of the dry layer and resonator displacements, we obtain an expression of the resonator displacement amplitude Z as:

$$Z = \frac{\omega_0^2}{(\omega^2 - \omega_0^2)} u_z \tag{27}$$

where $\omega_0 = \sqrt{K_0/M_0}$ is the angular resonant frequency of the mass-spring system. Note that, in the scenario of interest, surface waves wavelengths are much larger than the characteristic resonator spacing D. Hence, we can approximate the normal stress σ_{zz} exerted by the resonator at the surface ($z = 0$) as the elastic force of the resonator over the footprint area A:

$$\sigma_{zz}(z = 0) = \bar{\sigma}_{zz} = \frac{K_0}{A}(Z + u_z) \tag{28}$$

For a quadratic lattice arrangement, A is equal to D^2. Nonetheless, such effective medium approach is valid whether or not the resonators arrangement is regular [18], provided that the appropriate average footprint area A is used.

2.1.4. Dispersion relation

Equipped with a description of the wave motion in the dry layer, saturated half-space, and resonators array, the surface wave dispersion relation can be obtained by enforcing the boundary conditions at the surface of the soil $z = 0$:

$$(\sigma_{zz})_1 = (\bar{\sigma}_{zz})_1 \tag{29}$$

$$(\tau_{zx})_1 = 0 \tag{30}$$

and at the interface of the two layers $z = h$:

$$(\sigma_{zz})_1 = (\sigma_{zz})_2 \tag{31}$$

$$(\tau_{zx})_1 = (\tau_{zx})_2 \tag{32}$$

$$(u_x)_1 = (u_x)_2 \tag{33}$$

$$(u_z)_1 = (u_z)_2 \tag{34}$$

$$(p_f)_2 = 0 \tag{35}$$

in which the indexes 1 and 2 denote the upper layer and the bottom layer, respectively. As far as the interface between the dry and saturated layer is concerned, we here consider an open-pore scenario, i.e., a permeable interface at $z = h$. Hence, while the stresses and displacements are continuous at the interface, the pore pressure must vanish, as per Eq. (35).

Substituting Eqs. (7, 8, 23, 25, 27) into the seven boundary conditions (Eqs. 29-35) we obtain the system:

$$\begin{bmatrix} \mu_1\left(k^2+q^2\right)+p\Omega & 2i\mu_1 kq + ik\Omega & \mu_1\left(k^2+q^2\right)-p\Omega & -2i\mu_1 kq + ik\Omega & 0 & 0 & 0 \\ 2i\mu_1 kp & -\mu_1\left(k^2+q^2\right) & -2i\mu_1 kp & -\mu_1\left(k^2+q^2\right) & 0 & 0 & 0 \\ \mu_1\left(k^2+q^2\right)e^{-ph} & 2i\mu_1 kqe^{-qh} & \mu_1\left(k^2+q^2\right)e^{ph} & -2i\mu_1 kqe^{qh} & \xi_1 & \xi_2 & -2i\mu_2 kQ_3 \\ 2i\mu_1 kpe^{-ph} & -\mu_1\left(k^2+q^2\right)e^{-qh} & -2i\mu_1 kpe^{ph} & -\mu_1\left(k^2+q^2\right)e^{qh} & -2i\mu_2 kQ_1 & -2i\mu_2 kQ_2 & \mu_2\left(2k^2-k_S^2\right) \\ -ike^{-ph} & qe^{-qh} & -ike^{ph} & -qe^{qh} & ik & ik & -Q_3 \\ -pe^{-ph} & -ike^{-qh} & pe^{ph} & -ike^{qh} & Q_1 & Q_2 & ik \\ 0 & 0 & 0 & 0 & 1 & -\gamma & 0 \end{bmatrix} \begin{bmatrix} A_1 \\ A_2 \\ B_1 \\ B_2 \\ \widetilde{A}_1 \\ \widetilde{A}_2 \\ \widetilde{A}_3 \end{bmatrix} = \mathbf{0} \tag{36}$$

in which,

$$\xi_1 = (\lambda_2 + \alpha^2 M + \alpha M \delta_1)k_{P1}^2 - 2\mu_2 Q_1^2 \tag{37a}$$

$$\xi_2 = (\lambda_2 + \alpha^2 M + \alpha M \delta_2)k_{P2}^2 - 2\mu_2 Q_2^2 \tag{37b}$$

$$\gamma = -\frac{(\alpha+\delta_2)k_{P2}^2}{(\alpha+\delta_1)k_{P1}^2} \tag{37c}$$

$$\Omega = \frac{M_0\omega_0^2\omega^2}{A(\omega^2-\omega_0^2)} \tag{37d}$$

$$\widetilde{A}_j = \bar{A}_j e^{-Q_j h}, \quad (j = 1, 2, 3) \tag{37e}$$

Nontrivial solutions (k, ω) of Eq. (36) are found by imposing the determinant of the 7×7 matrix equal to zero, leading to the metasurface dispersion equation. As the closed-form solution of the system is not easily accessible, the *Newton-Raphson method* [32] is adopted in this paper to numerically compute the roots.

2.2. Limit cases: $kh \to \infty$ and $kh \to 0$

If the water table is sufficiently far away from the surface wave motion, namely in the short-wavelength regime $kh \to \infty$, the layered half-space can be reduced to a homogeneous single-phase soil by setting $B_1 = B_2 = \widetilde{A}_1 = \widetilde{A}_2 = \widetilde{A}_3 = 0$, so that Eq. (36) reduces to:

$$\begin{bmatrix} \mu_1(k^2+q^2)+p\Omega & 2i\mu_1 kq + ik\Omega \\ 2ikp & -(k^2+q^2) \end{bmatrix} \begin{bmatrix} A_1 \\ A_2 \end{bmatrix} = \mathbf{0} \tag{38}$$

Nontrivial solutions of Eq. (38) yields the dispersion relation for a metasurface laying on a single-phase elastic substrate and corresponds to equation 2 in Ref. [19]:

$$\left(2-\frac{c^2}{C_S^2}\right)^2-4\sqrt{\left(1-\frac{c^2}{C_P^2}\right)\left(1-\frac{c^2}{C_S^2}\right)}=\frac{c^2}{C_S^2}\frac{\Omega}{\mu_1 k}\sqrt{1-\frac{c^2}{C_P^2}} \tag{39}$$

Conversely, if the water table approaches the free surface or similarly in the long-wavelength limit (i.e., $kh \to 0$), Eq. (36), after some algebra, reduces to:

$$\begin{bmatrix} \mathbf{0} & \boldsymbol{\Delta}_{12} \\ \boldsymbol{\Delta}_{21} & \boldsymbol{\Delta}_{22} \end{bmatrix} \begin{bmatrix} \boldsymbol{y}_1 \\ \boldsymbol{y}_2 \end{bmatrix} = \mathbf{0} \tag{40}$$

in which the vectors $\boldsymbol{y}_1 = [A_1, A_2, B_1, B_2]^T$ and $\boldsymbol{y}_2 = [\widetilde{A}_1, \widetilde{A}_2, \widetilde{A}_3]^T$, and where:

$$\boldsymbol{\Delta}_{12} = \begin{bmatrix} -\xi_1 + Q_1\Omega & -\xi_2 + Q_2\Omega & 2i\mu_2 k Q_3 + ik\Omega \\ 2ikQ_1 & 2ikQ_2 & -2k^2 + k_S^2 \\ 1 & -\gamma & 0 \end{bmatrix} \tag{41a}$$

$$\boldsymbol{\Delta}_{21} = \begin{bmatrix} \mu_1\left(k^2+q^2\right)+p\Omega & 2i\mu_1 kq + ik\Omega & \mu_1\left(k^2+q^2\right)-p\Omega & -2i\mu_1 kq + ik\Omega \\ 2i\mu_1 kp & -\mu_1\left(k^2+q^2\right) & -2i\mu_1 kp & -\mu_1\left(k^2+q^2\right) \\ -ik & q & -ik & -q \\ -p & -ik & p & -ik \end{bmatrix} \tag{41b}$$

$$\boldsymbol{\Delta}_{22} = \begin{bmatrix} 0 & 0 & 0 \\ 0 & 0 & 0 \\ ik & ik & -Q_3 \\ Q_1 & Q_2 & ik \end{bmatrix} \tag{41c}$$

It is possible to show that the set of homogeneous equations $\boldsymbol{\Delta}_{12}\boldsymbol{y}_2 = \mathbf{0}$ corresponds to the boundary conditions at $z = 0$, i.e., $\sigma_{zz} = \bar{\sigma}_{zz}$, $\tau_{zx} = 0$ and $p_f = 0$ for a fully saturated half-space. This set of boundary conditions implicitly assumes that the whole resonator stress is discharged on the poroelastic medium skeleton, in other words, we assume that the open-pore condition is not influenced by the presence of the resonators. To obtain the nontrivial solutions of $\boldsymbol{\Delta}_{12}\boldsymbol{y}_2 = \mathbf{0}$, we impose:

$$|\boldsymbol{\Delta}_{12}| = \begin{vmatrix} -\xi_1 + Q_1\Omega & -\xi_2 + Q_2\Omega & 2i\mu_2 k Q_3 + ik\Omega \\ 2ikQ_1 & 2ikQ_2 & -2k^2 + k_S^2 \\ 1 & -\gamma & 0 \end{vmatrix} = 0 \tag{42}$$

which leads to the Rayleigh-wave dispersion of a metasurface placed on a saturated porous half-space. The equation above coincides with equation 16 in Ref. [31] when $\Omega = 0$, which provides the dispersion equation of Rayleigh waves in a bare saturated half-space.

3. Model and Validation

Before proceeding with any analytical investigations related to the influence of water table level and Biot's parameters on the dynamics of the metasurface, it is necessary to validate the obtained dispersion relation (Eq. 36) via numerical simulations. To this purpose, we develop a 2D plane-strain FE model, schematized in Fig. 2a, using Comsol Multiphysics. The software has a built-in $\boldsymbol{u} - p_f$ formulation to model the poroelastic fluid-solid interaction which is equivalent, under harmonic wave conditions [33], to the $\boldsymbol{u} - \boldsymbol{w}$ adopted on this work. The equivalence between the two formulations is proved in Appendix A. Following the approach in Ref. [34], we model the resonator in the unit cell using a point mass and a truss element (see Fig. 2a). The unit cell has a width $D = 1$ m and a depth $d = h + 6\lambda_R$, in which h is the water table and $\lambda_R = 2\pi c_R/\omega_0$ is the Rayleigh wavelength at the resonant frequency of the metasurface ω_0 (c_R is the Rayleigh wave velocity in the saturated layer). Bloch boundary conditions are imposed on the left and right edges of the cell to simulate an infinite array of resonators along the wave propagation direction. Clamped boundary conditions are applied to the bottom edge to avoid undesired rigid motions. The Young's modulus of the truss is $E = M_0\omega_0^2/S$, where S is the cross-sectional area of the truss. The substrate domain is discretized into quadrilateral elements with quadratic Lagrange shape functions. The minimum mesh dimension is smaller than $D/15$ and is sufficient to obtain a convergent solution at the highest frequency of interest.

Assuming the mechanical parameters in Table 1 and an ideal fluid with viscosity $\eta = 0$, we calculate numerically (as solution of Eq. 36) and via FE the dispersion curves for vertically polarized surface waves in a bi-layer system, with a water table at $h = 20$ m (see Fig. 2a). Note that FE surface wave solutions are selected from the whole set of Bloch modes utilizing the post-processing technique in Ref. [35].

A first insight on the main features of the analytical dispersion curve suggests that the presence of the water table has minor effects on the coupling between Rayleigh waves and the metasurface (see Fig. 2b). In fact, similarly to what observed in a fully elastic half-space, the metasurface resonance couples with the Rayleigh mode, showing an "avoided-crossing" behavior which results in a surface wave band-gap. This dynamics is confirmed by the FE solutions which agree well with the analytical results.

We also display the displacement field in the soil and the pressure field in the fluid for a representative mode shape extracted at $k = 0.35$ rad/m along the lowest order branch. The displacement field is confined in the vicinity of the free surface; similarly, the pore pressure is concentrated near the water table. Again, the FE solution (Fig. 2c) agrees well with the associated analytical prediction (Fig. 2d). An extended investigation on the metasurface dispersive features and on their dependence on key porous mechanical parameters and water table level is conducted in the next section, leveraging the validated analytical framework.

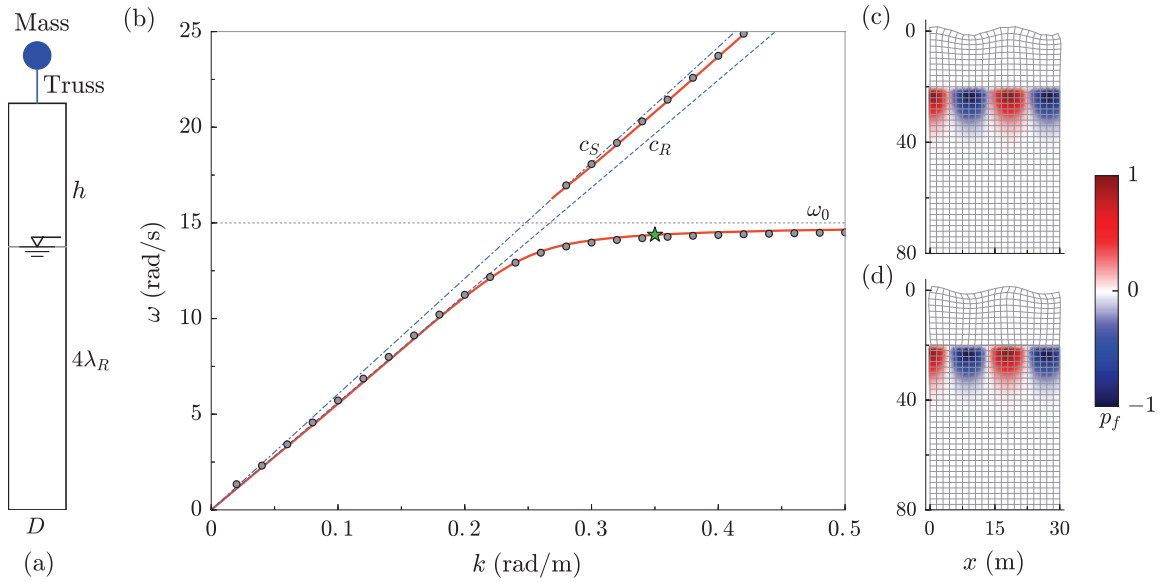

Fig. 2. Comparative analytical vs FEM study. (a) Unit cell used for dispersion relation calculations. (b) Dispersion curves for a bi-layer system coupled with the metasurface: comparison between the analytical formulation (denoted by solid lines) and the FE model (denoted by circles). (c) FE and (d) analytical mode shapes computed at $k = 0.35$ (highlighted with a star in Fig. 2b). The colormap denotes the normalized pore pressure.

Table 1: Mechanical parameters of metasurface and poroelastic substrate. Some of the poroelastic parameters are taken from Ref. [36].

Parameter	Value
Resonator mass, M_0	1000 kg
Angular resonant frequency, ω_0	15 rad/s
Lattice spacing, D	1 m
Porosity, ϕ_1, ϕ_2	0.25
Tortuosity, τ_∞	2
Permeability, κ	10^{-11} m^2
Viscosity of fluid, η	$0 \sim 10^{-4}$ Pa·s
Density of grains, ρ_{s1}, ρ_{s2}	2533 kg/m^3
Mass density of fluid, ρ_f	1000 kg/m^3
Bulk modulus of fluid, K_f	2 GPa
Bulk modulus of grains, K_s	222.2 MPa
Young modulus of skeleton, E_1, E_2	20 MPa
Poisson ratio of skeleton, ν_1, ν_2	0.35

4. Results

In this section, two scenarios of interest are investigated, namely, a metasurface laying on a saturated half-space (i.e., water table at $h = 0$) and a metasurface laying on a porous layered system (i.e., water table at $h \neq 0$). The study of the first configuration aims at: (i) singling out the influence of two key parameters, namely tortuosity and viscosity, on the surface waves dispersion properties; (ii) unveiling a surface wave attenuation

mechanism germane of a saturated porous substrate. The analyses on the dry-saturated layered configurations are instead conducted to understand the effect of the water table level on the wave conversion mechanism of Rayleigh waves.

4.1. Saturated porous half-space

In absence of the metasurface, a single Rayleigh mode can be found in a saturated poroelastic half-space modeled according to Biot's theory [31]. When an ideal fluid is considered, this surface mode is purely propagative, i.e., characterized by a null attenuation, non-dispersive, and its velocity of propagation can be found by solving Eq. (42) for $\Omega = 0$. Variations of tortuosity and/or fluid viscosity within typical ranges for saturated porous soils have a minor influence on the dispersive properties of Rayleigh waves. Tortuosity, in fact, is a purely geometrical factor that describes the microscopic geometry of the skeleton and the distribution of pores; high values of tortuosity reflect a complex wave path through the porous material, which in turn yields a lower velocity of propagation of the bulk P2 wave only. Fluid viscosity, instead, causes large energy dissipation and dispersion of P2 waves, whereas marginally affects P1 and S waves.

With these premises, we can now investigate the effect of tortuosity and viscosity on the dispersive properties of the metasurface. At first, we calculate the metasurface dispersion properties considering an ideal fluid, i.e., null viscosity, and keeping the other parameters the same as those in Table 1. The real dispersion curve for two distinct values of tortuosity, ($\tau_\infty = 1.2 - 2.8$), selected within the characteristic range of values of tortuosity in soils ($1 \sim 3$ [36]) are shown in Fig. 3a, b. The hybridized Rayleigh-wave modes, which are solutions of Eq. (42), are marked with blue circles; pressure ($\omega = c_{P1}k$, $\omega = c_{P2}k$) and shear ($\omega = c_S k$) wave solutions are drawn as dashed lines, red and black, respectively. Rayleigh waves in the bare saturated half-space are reported, as reference, with continuous black line. As observed in single-phase elastic medium, the local resonances couple with the Rayleigh mode yielding two repelling branches, which separate around the metasurface resonance leaving a surface wave band-gap. The cut-on frequency of the upper branch, laying at the intersection between the upper hybrid mode and the shear wave line (see Fig. 3a), marks the upper edge of the band gap.

Through comparison between Figs. 3a and b, we observe that the tortuosity has no significant influence on the hybridization phenomenon. Conversely, as anticipated in the premises, a major change in the phase velocity of the P2 wave is observed. In particular, it is possible to calculate a critical value of tortuosity, $\widetilde{\tau}_\infty = 2.4$ for the considered example, for which the phase velocities c_{P2} and c_S coincide. The value $\widetilde{\tau}_\infty$ marks the occurrence of a more complex scenario, which characterizes all the porous substrates with $\tau_\infty > \widetilde{\tau}_\infty$, or equivalently $c_{P2} < c_S$. In these cases, in addition to the hybridization band gap, we observe a frequency range where $c_{P2} < c < c_S$ (see light blue region highlighted in Fig. 3b). Within this frequency range surface modes are characterized by complex wavenumbers Q_2, (cf. potential functions assumed in Eq. (20)). As a result, part of the surface wave energy is leaked as a P2 wave within the bulk. Note that the extension of this frequency range increases with an increase in tortuosity (see Fig. 3c). The energy leakage results in a non-null attenuation (k_i) of the surface wave along the propagation direction (see Fig. 3d)

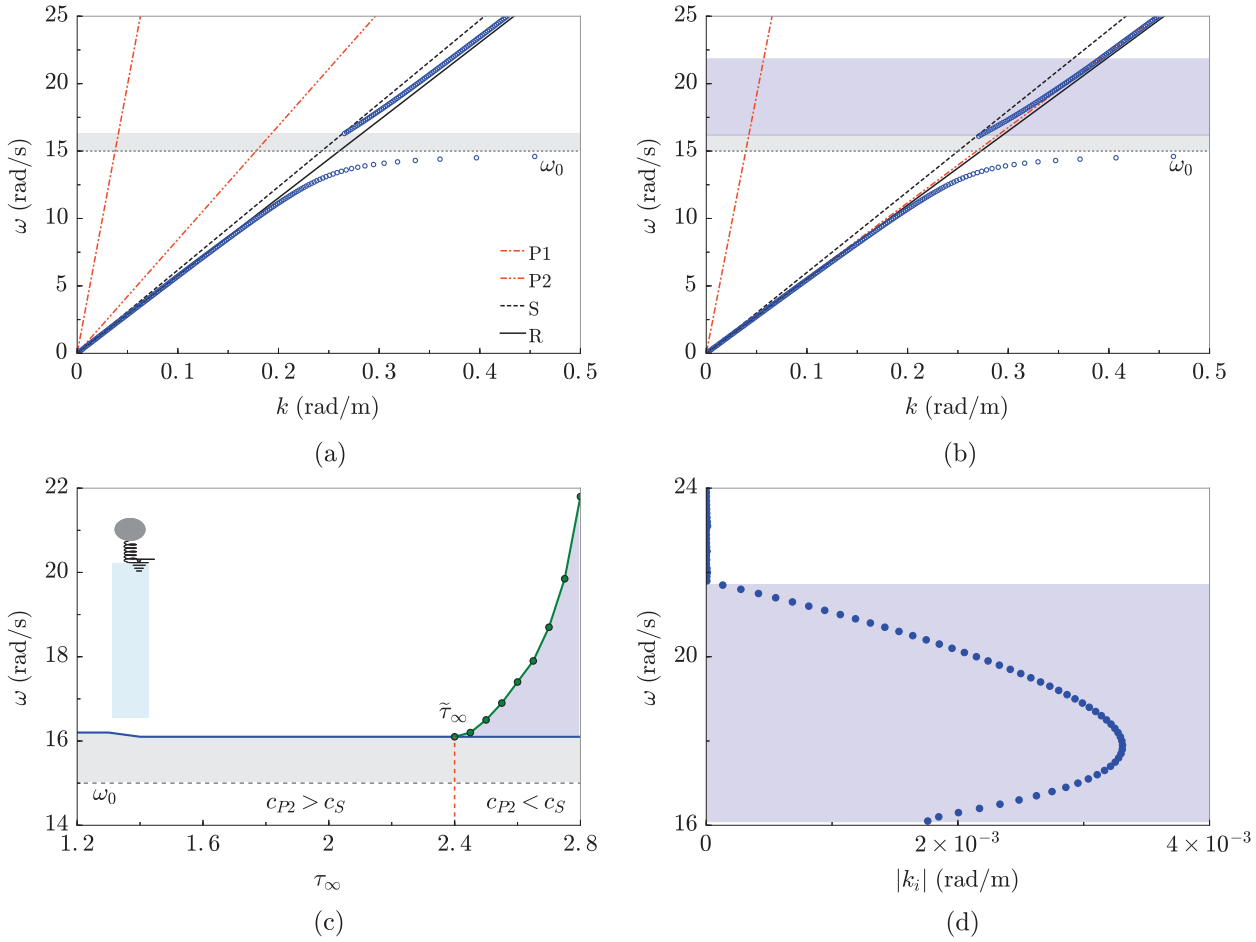

Fig. 3. Influence of tortuosity τ_∞ on the propagation of surface waves in a fully saturated soil system coupled with a metasurface: (a) Dispersion curve for $\tau_\infty = 1.2$. (b) Dispersion curve for $\tau_\infty = 2.8$. (c) Band gap width (grey box) and P2-wave leakage (light blue box) for different values of tortuosity. (d) Rayleigh wave attenuation due to P2-wave leakage for $\tau_\infty = 2.8$.

To evidence this novel feature introduced by the fluid-solid interaction, we carry out FE numerical simulations considering a fully saturated porous half-space, i.e., a water table level $h = 0$. A metasurface with 300 resonators, arranged as in Fig. 4, is placed on the free surface. The incident surface waves are excited by a harmonic point load sufficiently far away from the metasurface. Perfectly Matched Layers (PMLs) are applied to the vertical and bottom edges of the model to mimic the half-space and avoid unwanted reflected components.

Fig. 5a shows the normalized displacement wavefield produced by an incident Rayleigh wave with angular frequency $\omega = 15.5$ rad/s in a saturated half-space characterized by a value of tortuosity $\tau_\infty = 1.2$. As expected, the surface wave is converted to a downward shear bulk waves, following the prediction given by the dispersion curve in Fig. 3a. The same phenomenon can be observed for the half-space with a tortuosity $\tau_\infty = 2.8$, as shown in Fig. 5b.

Conversely, the propagation of P2 waves occurs only in saturated substrates with $\tau_\infty > 2.4$, as evidenced by comparing the normalized pore pressure fields in Fig. 6a and 6b, calculated via harmonic simulations at $\omega = 18$ rad/s for two substrates with $\tau_\infty = 1.2$ and $\tau_\infty = 2.8$, respectively.

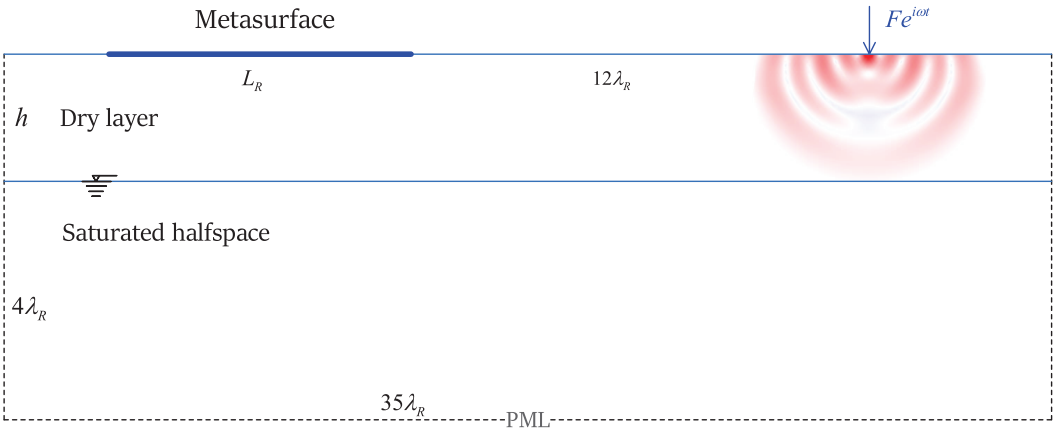

Fig. 4. Schematic of the model geometry.

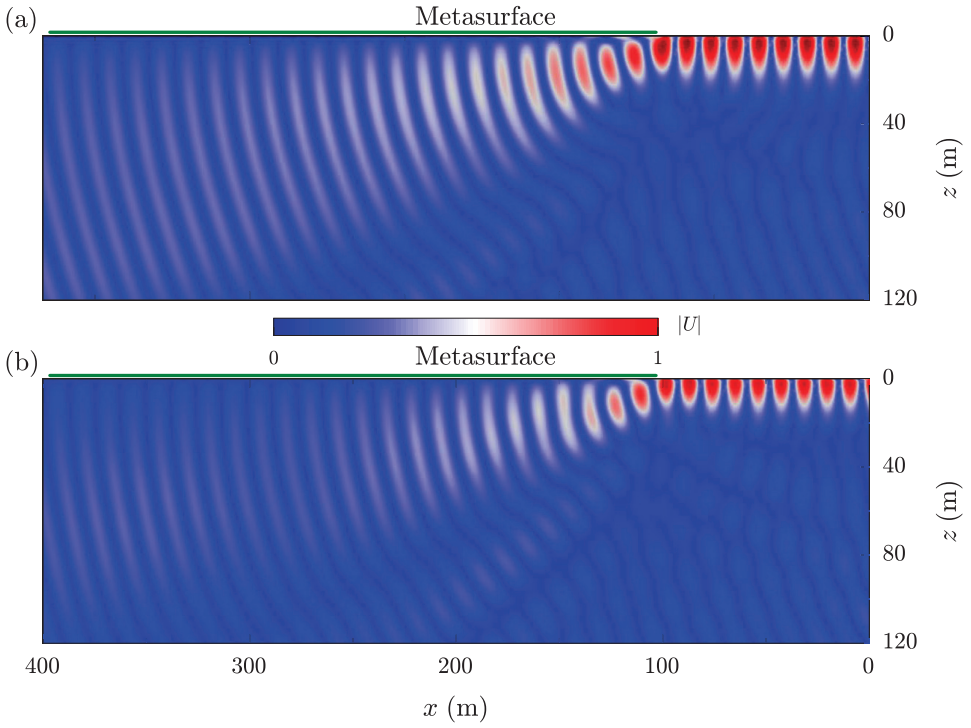

Fig. 5. Normalized total displacement of the skeleton for a harmonic simulation at $\omega = 15.5$ rad/s. (a) $\tau_\infty = 1.2$. (b) $\tau_\infty = 2.8$.

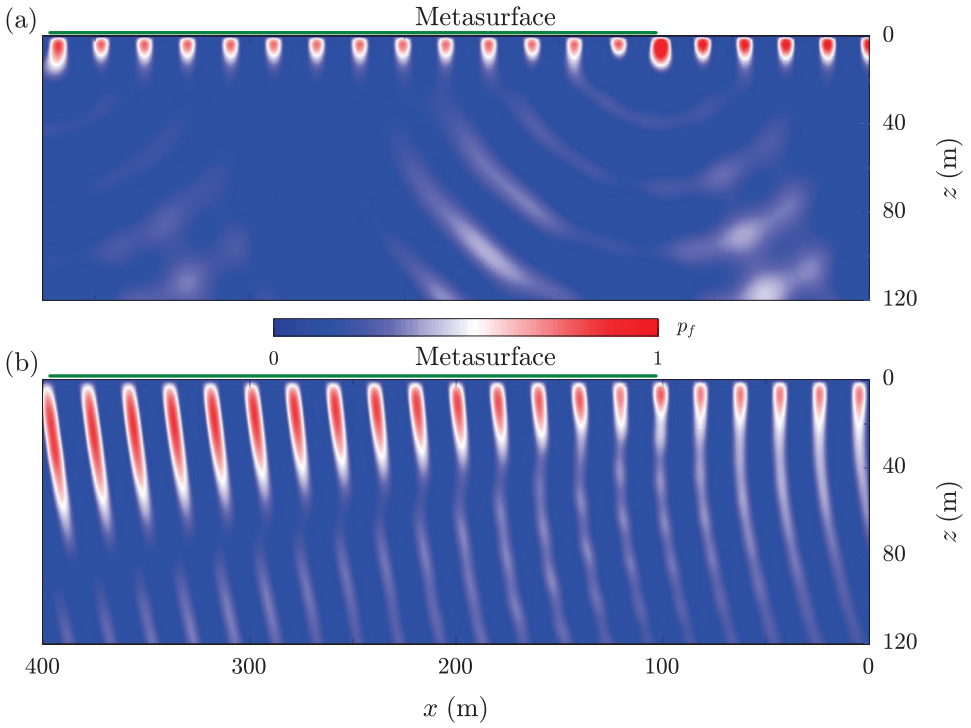

Fig. 6. Normalized pore pressure for a harmonic simulation at $\omega = 18$ rad/s. (a) $\tau_\infty = 1.2$. (b) $\tau_\infty = 2.8$.

We now move our investigation to the effects of fluid viscosity on the metasurface dispersive properties. As a first example, we select a value of tortuosity $\tau_\infty = 2.8$ and two values of viscosity $\eta = [10^{-6}, 10^{-2}]$ Pa·s, keeping unchanged the other mechanical parameters (i.e., data in Table 1). By comparing the real dispersion curves of the two viscous cases displayed in Fig. 7a, no significant changes are found in the hybridization phenomenon. Conversely, as regards to the attenuation curve (k_i vs. ω) in Fig. 7b, we observe that the absolute value of k_i is larger for the lowest chosen value of viscosity ($\eta = 10^{-6}$ Pa·s), except for frequencies close to ω_0, where a larger viscosity results in a larger attenuation. To explain this counter-intuitive result, we compare the variation of k_i with η for hybrid Rayleigh waves and shear waves at a given angular frequency. While for the Rayleigh wave we use the dispersion relation Eq. (42) to compute k_i for different values of η, for the S wave, we derive the following closed-form relation:

$$k_i = -\frac{\rho_f^2}{2\mu_2}\frac{\omega}{k_r}\frac{\omega^2\eta\kappa}{\left(\tau_\infty\kappa\omega\rho_f/\phi\right)^2 + \eta^2} \tag{43}$$

which is obtained via algebraic manipulation of Eq. (19).

Figure 7c reports the variation of k_i vs. η for $\omega = 10$ rad/s where the solutions for S waves are drawn as a solid line, and those for hybrid Rayleigh waves are marked with circles. Interestingly, surface waves travelling within the metasurface and shear waves present a similar k_i vs η trend, with a maximum attenuation (i.e., a minimum value of k_i) found at a given and finite value of viscosity, here labelled as η_{max}. For S waves the viscosity value which minimizes Eq. (43) for a given angular frequency ω is:

$$\eta_{max,S}(\omega) = \frac{\tau_\infty\kappa\rho_f}{\phi}\omega \tag{44}$$

Conversely, for hybrid Rayleigh waves the viscosity $\eta_{max,hR}(\omega)$ is found via numerical solutions of Eq. (42), performing a larger parametric study in the range $\eta = [0 \sim 1.0 \times 10^{-4}]$ Pa·s. The results of this parametric analysis are displayed in Fig. 7d, where $\eta_{max,hR}(\omega)$ values are marked by colored dots, together with values of $\eta_{max,S}(\omega)$ marked as a solid line. Note that S and hybrid Rayleigh waves show similar trends for the whole frequency range of interest $[0 \sim 25]$ rad/s, apart from frequencies close to resonance ω_0 where $\eta_{max,hR}(\omega)$ is not bounded, i.e., the larger the viscosity the larger the attenuation. Such a result can be ascribed to the localization of wave energy at the free surface, which in turn maximizes the wave attenuation for larger values of viscosity.

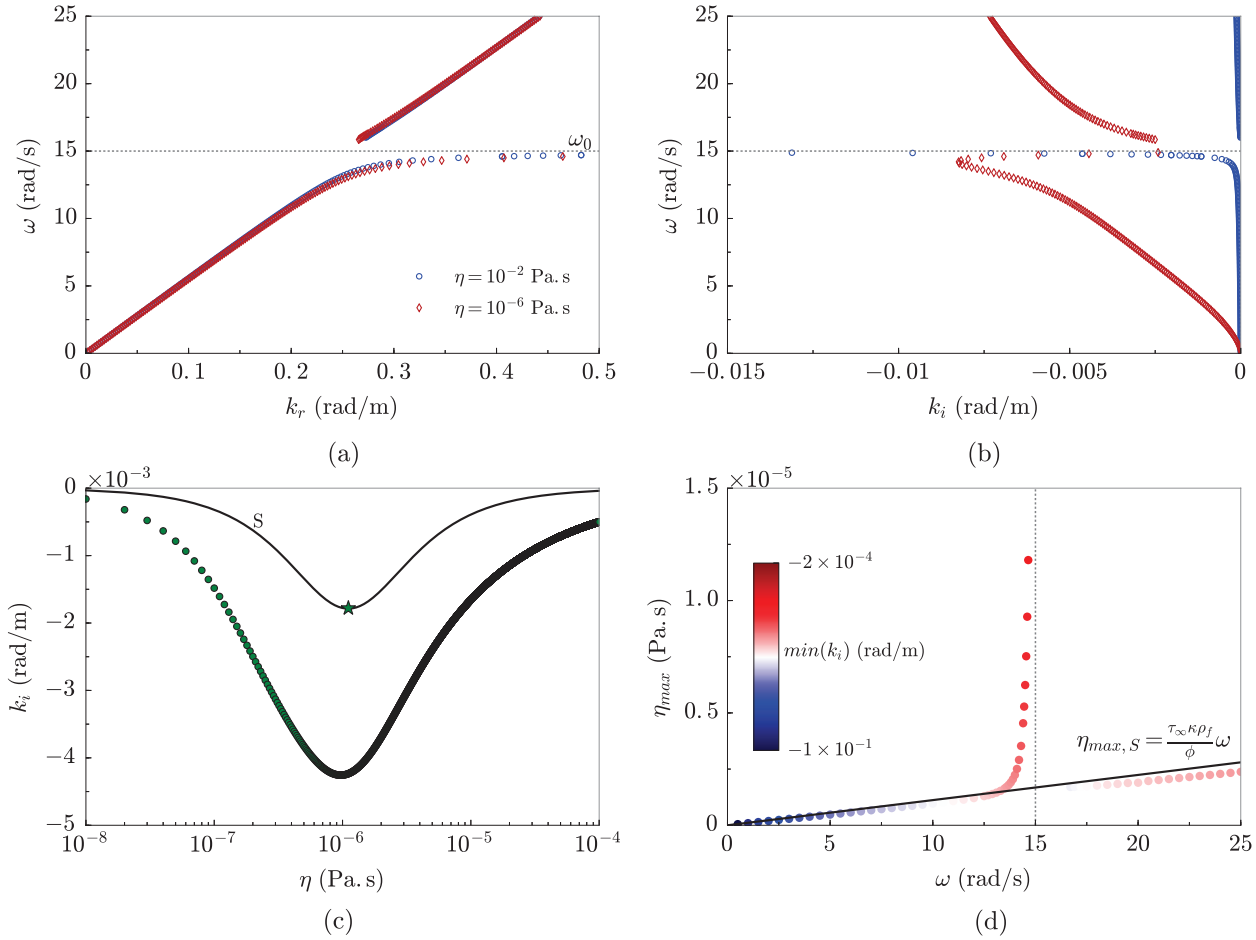

Fig. 7. Influence of the fluid viscosity η ($\tau_\infty = 2.8$): (a) Real dispersion curves for $\eta = [10^{-6}, 10^{-2}]$ Pa·s. (b) Attenuation curves for $\eta = [10^{-6}, 10^{-2}]$ Pa·s. (c) Shear and Rayleigh wave attenuation vs. fluid viscosity at $\omega = 10$ rad/s. (d) Fluid viscosity (η_{max}) which maximizes S and Rayleigh wave attenuation at given frequency ω. The solid line denotes the analytical solutions for S waves, while colored dots indicate the numerical solutions for hybrid Rayleigh waves. The color map indicates the corresponding value of attenuation.

4.2. Layered porous soil

We now move our investigation to a substrate stratigraphy with a water table level h located at a given and finite depth from the soil surface. For the sake of simplicity, we restrict our analysis to the case of an ideal fluid, having in mind that a non-null value of viscosity would mainly affect the imaginary part of the dispersion curve. Similarly, we conduct our investigation assuming a fixed value of tortuosity $\tau_\infty = 2.8$, and all the other mechanical parameters as collected in Table 1.

We start by considering a water table level $h = 5$ m, hence smaller than the Rayleigh wavelength in dry soil at the main frequency of interest (i.e., $\lambda = 24$ m at ω_0). As for the dispersion curve of a metasurface laying on a fully saturated porous half-space, the fundamental branch bends off to approach the resonance frequency ω_0 asymptotically (Fig. 8a), leaving a band gap where surface-to-bulk wave conversion is expected. The conversion from Rayleigh waves to downward bulk waves (Fig. 8b) occurs with no significant reflections at the dry layer-saturated half-space interface, as evidenced by the wavefield obtained via FE harmonic simulations at $\omega = 15.1$ rad/s. No significant changes are found when the water table is higher than the wavelength of interest, e.g., $h = 30$ m, as shown by the metasurface dispersion curve (Fig. 8c) and the associated harmonic simulations (Fig. 8d).

A more complex scenario emerges when the presence of water is accompanied by a change in the mechanical properties between the dry and saturated layers. As an example, we here consider a variation in porosity between the dry and saturated soil, a condition commonly found in real sites. In particular, we assume $\phi_1 = 0.1$, $\phi_2 = 0.25$, $\tau_\infty = 2.8$, $h = 30$ m, keeping all the other parameters mechanical parameters as in Table 1. The variation in porosity leads to different bulk wave velocities within the two layers. As a result, multiple surface modes are found with increasing frequency. Such modes result from the interaction of P and S waves at both the traction-free boundary and the contact interface of the layers. Differently from the fundamental mode which hybridizes with the metasurface resonances, we note that the second-order mode (see Fig. 8e) extends below ω_0, suggesting that the band gap and the related surface-to-shear conversion may vanish. To confirm this result, we carry out numerical simulations at $\omega = 15.1$ rad/s. The calculated wavefield, displayed in Fig. 8g,

shows that incident Rayleigh mode initially redirected within the bulk, eventually evolves into a more complex wavefield reflected at the layer interface and then channeled below the metasurface as a higher-order surface mode. This higher mode (see Fig. 8f), presents a null surface displacement, a feature already experimentally and numerically observed for higher-order surface modes traveling through metasurfaces embedded in a dry granular medium [37, 38].

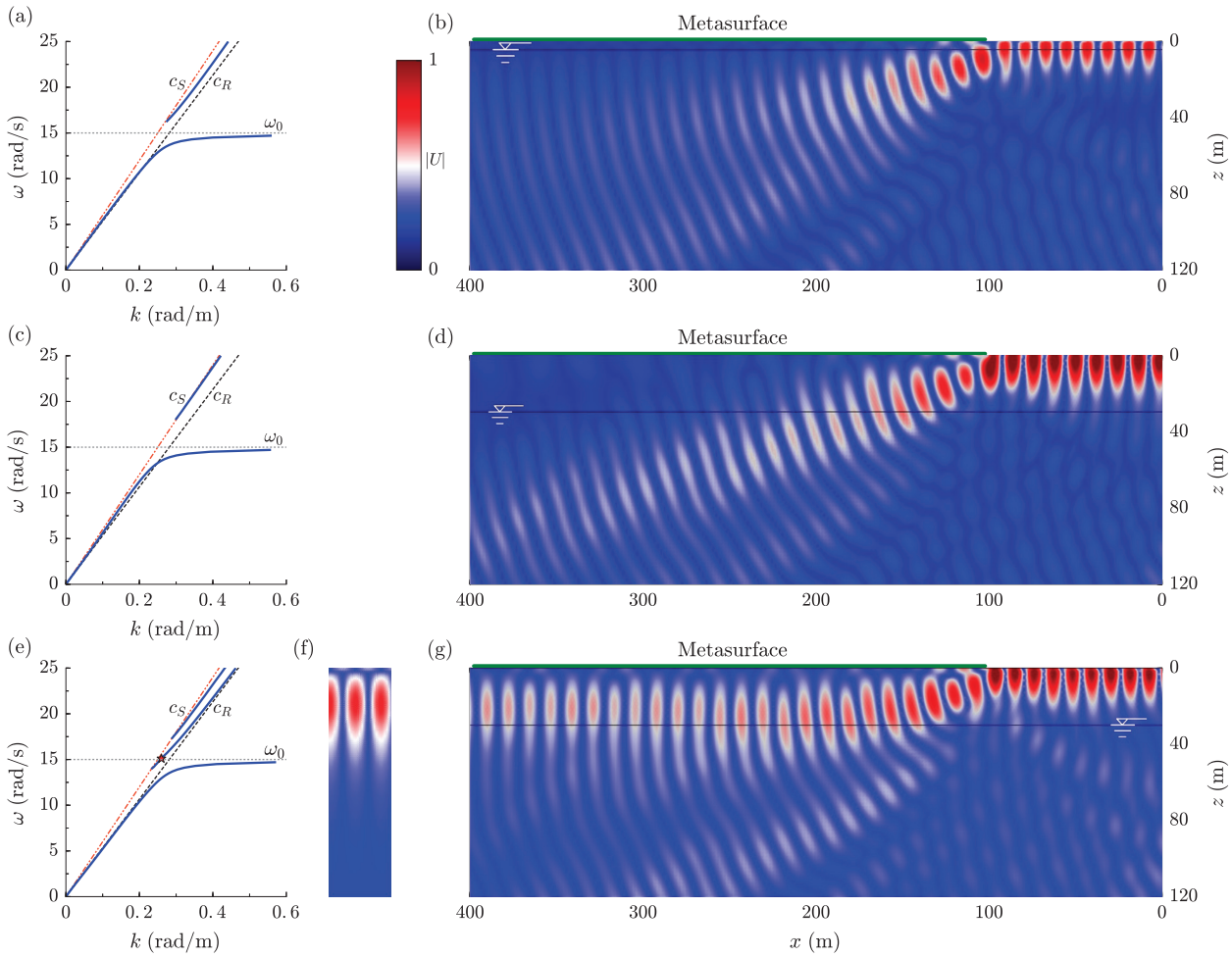

Fig. 8. Influence of the water table and porosity: (a) Dispersion curves for $h = 5$ m, $\phi_1 = \phi_2 = 0.25$. (b) Normalized total displacement of the skeleton for $h = 5$ m. (c) Dispersion curves for $h = 30$ m, $\phi_1 = \phi_2 = 0.25$. (d) Normalized total displacement of the skeleton for $h = 30$ m. (e) Dispersion curves for $h = 30$ m, $\phi_1 = 0.1$, $\phi_2 = 0.25$. (f) The eigenmode at the star point ($\omega = 15.1$ rad/s). (g) Normalized total displacement of the skeleton for $h = 30$ m. All simulations are at $\omega = 15.1$ rad/s.

5. Conclusions and Discussions

The recent surge of metamaterials [39] and metasurfaces developed for seismic wave control motivates the derivation of analytical models [17, 21, 40] able to capture the interaction of bulk and surface waves with structured and resonant surface devices. Within this context, our work provides a novel element of interest, considering the propagation of surface waves through a porous layered saturated medium. This additional complexity is required to better replicate soil configuration typically encountered in civil engineering practice, where the water table level can be located at a finite depth below the surface.

Our model is developed by exploiting a Biot's description of the porous layer and an effective medium description of the metasurface dynamics, so as to derive the dispersive properties of Rayleigh waves propagating in fully saturated or layered porous media equipped with surface mass-spring resonators. The obtained framework allows unveiling the fundamental dynamics introduced by the fluid-solid interaction within the porous substrate.

In particular, we found that within certain frequency ranges, the incident Rayleigh waves leak part of their energy into the substrate as downward propagating slow pressure waves (P2), a mechanism that attenuates the overall energy conveyed at the surface. This phenomenon is accompanied by the "classical" surface-to-shear wave conversion, previously observed in metasurfaces over an elastic substrate, which occurs due to the hybridization between Rayleigh waves and metasurface resonances. By leveraging our analytical framework, we investigated how these peculiar effects are influenced by some key mechanical parameters like tortuosity, viscosity, and water table level. We found that energy leakage occurs only when the P2 wave velocity lower

than S wave one. This condition is met only for specific value of tortuosity. Additionally, by exploiting the proportionality between Rayleigh and S wave velocities, we found that the value of viscosity which maximizes the surface wave attenuation changes for different frequency regime. In particular, we showed that this value of viscosity is bounded except for frequency close to the metasurface resonance.

Finally, we found that the water table level has a minor influence on both the surface wave band gap extension and on the related surface-to-bulk waves conversion. Conversely, when the presence of water is accompanied by a change in the porosity between the dry and the saturated layer, the converted S waves can be partially back-reflected at the layer interface. The reflected waves can, in turn, excite higher-order surface modes that remain confined below the surface. These results suggest further investigations to define the existence and extension of "screened/mitigated" zones for future realization of wave barriers and vibration mitigation systems in layered saturated soils.

Overall, we expect that our theoretical framework will serve as a guide to better interpret data from experimental or numerical tests on engineered resonant structures, and by analogy, on forest of trees [41] or densely-built environments [42] interacting with surface ground motions in saturated soils.

Appendix A. Equivalence between $\boldsymbol{u-w}$ and $\boldsymbol{u-p_f}$ Biot's formulations

In this Appendix we show that the dispersion relation for Rayleigh waves existing in a Biot's soil, obtained in this work by using $\boldsymbol{u}-\boldsymbol{w}$ variables as in Eq. (36), can be identically obtained by using the $\boldsymbol{u}-p_f$ variables.

Let us recall the governing equations for a poroelastic medium. Assuming a time-harmonic variation of the skeleton displacement field $\boldsymbol{u}(\boldsymbol{x},t)=\boldsymbol{u}(\boldsymbol{x})e^{i\omega t}$ and of the relative fluid-solid displacement field $\boldsymbol{w}(\boldsymbol{x},t)=\boldsymbol{w}(\boldsymbol{x})e^{i\omega t}$, according to the Biot's $\boldsymbol{u}-\boldsymbol{w}$ formulation in Eq. (9), the governing equations for a poroelastic medium reduce to:

$$(\lambda_2+\mu_2)\nabla(\nabla\cdot\boldsymbol{u})+\mu_2\nabla^2\boldsymbol{u}-\alpha\nabla p_f+\rho\omega^2\boldsymbol{u}+\rho_f\omega^2\boldsymbol{w}=\boldsymbol{0} \tag{A.1a}$$

$$-\nabla p_f+\rho_f\omega^2\boldsymbol{u}+\rho_c\omega^2\boldsymbol{w}=\boldsymbol{0} \tag{A.1b}$$

where the pore pressure reads:

$$p_f=-\alpha M\nabla\cdot\boldsymbol{u}-M\nabla\cdot\boldsymbol{w} \tag{A.2}$$

From Eq. (A.1b) we can write the relative displacement $\boldsymbol{w}$ as:

$$\boldsymbol{w}=\frac{1}{\omega^2\rho_c}(\nabla p_f-\rho_f\omega^2\boldsymbol{u}) \tag{A.3}$$

Substituting Eq. (A.3) into Eq. (A.1a) and taking the divergence of Eq. (A.1b), the governing equations, i.e., Eqs. (A.1a) and (A.1b), can be written as a function of $\boldsymbol{u}$ and p_f [43]:

$$(\lambda_2+\mu_2)\nabla(\nabla\cdot\boldsymbol{u})+\mu_2\nabla^2\boldsymbol{u}+\omega^2\left(\rho-\frac{\rho_f^2}{\rho_c}\right)\boldsymbol{u}-\left(\alpha-\frac{\rho_f}{\rho_c}\right)\nabla p_f=\boldsymbol{0} \tag{A.4a}$$

$$\omega^2(\rho_f-\alpha\rho_c)\nabla\cdot\boldsymbol{u}-\nabla^2 p_f-\frac{\rho_c\omega^2}{M}p_f=0 \tag{A.4b}$$

The Eqs. (A.4) provide the $\boldsymbol{u}-p_f$ formulation of the Biot's wave theory.

At this stage, by employing the Helmholtz decomposition of the potential functions (Eq. (11)) in Eqs. (A.2) and (A.4), we obtain:

$$\left\{\begin{bmatrix}\lambda_2+2\mu_2+\alpha^2M & \alpha M\\ \alpha M & M\end{bmatrix}\nabla^2+\omega^2\begin{bmatrix}\rho & \rho_f\\ \rho_f & \rho_c\end{bmatrix}\right\}\begin{Bmatrix}\Phi_s\\ \Phi_f\end{Bmatrix}=\boldsymbol{0} \tag{A.5}$$

and,

$$\mu_2\nabla^2\Psi_{sy}+\omega^2\left(\rho-\frac{\rho_f^2}{\rho_c}\right)\Psi_{sy}=0 \tag{A.6}$$

Eqs. (A.5) and (A.6) describe the propagation of P and S bulk waves in a saturated medium, respectively. In particular, Eq. (A.5) is identical to the characteristic equation of P waves obtained via $\boldsymbol{u}-\boldsymbol{w}$ formulation (see Eq. (15)). Similarly the scalar Eq. (A.6) yields the same root as Eq. (19) obtained via the $\boldsymbol{u}-\boldsymbol{w}$ formulation. Note that in the $\boldsymbol{u}-p_f$ formulation only the Ψ_{sy} component of the vector potential is required to formulate the governing equation of shear waves.

Exploiting the $\boldsymbol{u} - p_f$ description of bulk waves in a poroelastic medium, we can tackle the derivation of surface waves in a saturated half-space. For this purpose we assume the following potentials:

$$\Phi_s = \left(\bar{A}_1 e^{-Q_1 z} + \bar{A}_2 e^{-Q_2 z}\right) e^{i(\omega t - kx)} \tag{A.7a}$$

$$\Phi_f = \left(\bar{A}_1 \delta_1 e^{-Q_1 z} + \bar{A}_2 \delta_2 e^{-Q_2 z}\right) e^{i(\omega t - kx)} \tag{A.7b}$$

$$\Psi_{sy} = \bar{A}_3 e^{-Q_3 z} e^{i(\omega t - kx)} \tag{A.7c}$$

By substituting Eqs. (A.7) into the elastic constitutive relations, we have:

$$\begin{aligned}
\sigma_{zz} &= (\lambda_2 + \alpha^2 M)\nabla^2 \Phi_s + \alpha M \nabla^2 \Phi_f + 2\mu_2 \left(\frac{\partial^2 \Phi_s}{\partial z^2} + \frac{\partial^2 \Psi_{sy}}{\partial x \partial z} \right) \\
&= \left[-\left(\lambda_2 + \alpha^2 M + \alpha M \delta_1\right) k_{P1}^2 + 2\mu_2 Q_1^2 \right] \bar{A}_1 e^{-Q_1 z} e^{i(\omega t - kx)} \\
&+ \left[-\left(\lambda_2 + \alpha^2 M + \alpha M \delta_2\right) k_{P2}^2 + 2\mu_2 Q_2^2 \right] \bar{A}_2 e^{-Q_2 z} e^{i(\omega t - kx)} \\
&+ 2i\mu_2 k Q_3 \bar{A}_3 e^{-Q_3 z} e^{i(\omega t - kx)}
\end{aligned} \tag{A.8a}$$

$$\begin{aligned}
\tau_{zx} &= 2\mu_2 \frac{\partial^2 \Phi_s}{\partial x \partial z} + \mu_2 \left(\frac{\partial^2 \Psi_{sy}}{\partial x^2} - \frac{\partial^2 \Psi_{sy}}{\partial z^2} \right) \\
&= \mu_2 \left[2ikQ_1 \bar{A}_1 e^{-Q_1 z} + 2ikQ_2 \bar{A}_2 e^{-Q_2 z} - (2k^2 - k_S^2) \bar{A}_3 e^{-Q_3 z} \right] e^{i(\omega t - kx)}
\end{aligned} \tag{A.8b}$$

$$\begin{aligned}
p_f &= -M(\alpha \nabla^2 \Phi_s + \nabla^2 \Phi_f) \\
&= M \left[(\alpha + \delta_1) k_{P1}^2 \bar{A}_1 e^{-Q_1 z} + (\alpha + \delta_2) k_{P2}^2 \bar{A}_2 e^{-Q_2 z} \right] e^{i(\omega t - kx)}
\end{aligned} \tag{A.8c}$$

The expressions of normal and tangential stresses as well as pore pressure obtained from the $\boldsymbol{u} - p_f$ formulation, are identical to the corresponding ones in Eq. (25) obtained via the $\boldsymbol{u} - \boldsymbol{w}$ formulation. As a result, the use of the $\boldsymbol{u} - p_f$ formulation leads to the same characteristic equation, i.e. the dispersion relation described in Eq. (36).

We recognize that for our problem the two formulations of the Biot's model are equivalent and no major simplifications belong to one or the other formulation. Still, we remark that in scenarios where an impermeable condition at the interface between the dry and the saturated layer is considered, the use of a $\boldsymbol{u} - \boldsymbol{w}$ formulation is advisable, since it naturally allows to impose a null normal component of the relative fluid displacement at the impermeable interface [26].

Acknowledgments

This project has received funding from the European Union's Horizon 2020 research and innovation programme under the Marie Skłodowska Curie grant agreement No 813424. A.P. acknowledges the support of the University of Bologna - DICAM through the research fellowship "Metamaterials for seismic waves attenuation". Z.C. and Z.S. acknowledge the support of the National Natural Science Foundation of China (51878030, 51878031) and the Beijing Natural Science Foundation (8182045).

Conflict of interest

The authors declare that they have no conflict of interest.

References

[1] D. R. Smith, J. B. Pendry, M. C. Wiltshire, Metamaterials and negative refractive index, Science 305 (5685) (2004) 788–792.

[2] M. Maldovan, Sound and heat revolutions in phononics, Nature 503 (7475) (2013) 209–217.

[3] M. I. Hussein, M. J. Leamy, M. Ruzzene, Dynamics of phononic materials and structures: Historical origins, recent progress, and future outlook, Applied Mechanics Reviews 66 (4) (2014) 1–38.

[4] Z. Liu, X. Zhang, Y. Mao, Y. Zhu, Z. Yang, C. T. Chan, P. Sheng, Locally resonant sonic materials, Science 289 (5485) (2000) 1734–1736.

[5] H. Huang, C. Sun, G. Huang, On the negative effective mass density in acoustic metamaterials, International Journal of Engineering Science 47 (4) (2009) 610–617.

[6] Y. Pennec, J. O. Vasseur, B. Djafari-Rouhani, L. Dobrzyński, P. A. Deymier, Two-dimensional phononic crystals: Examples and applications, Surface Science Reports 65 (8) (2010) 229–291.

[7] F. Casadei, T. Delpero, A. Bergamini, P. Ermanni, M. Ruzzene, Piezoelectric resonator arrays for tunable acoustic waveguides and metamaterials, Journal of Applied Physics 112 (6) (2012) 064902.
[8] K. H. Matlack, A. Bauhofer, S. Krödel, A. Palermo, C. Daraio, Composite 3d-printed metastructures for low-frequency and broadband vibration absorption, Proceedings of the National Academy of Sciences 113 (30) (2016) 8386–8390.
[9] M. Yang, P. Sheng, Sound absorption structures: From porous media to acoustic metamaterials, Annual Review of Materials Research 47 (2017) 83–114.
[10] Z. Cheng, Z. Shi, Composite periodic foundation and its application for seismic isolation, Earthquake Engineering & Structural Dynamics 47 (4) (2018) 925–944.
[11] F. Basone, M. Wenzel, O. S. Bursi, M. Fossetti, Finite locally resonant metafoundations for the seismic protection of fuel storage tanks, Earthquake Engineering & Structural Dynamics 48 (2) (2019) 232–252.
[12] A. Franchini, O. S. Bursi, F. Basone, F. Sun, Finite locally resonant metafoundations for the protection of slender storage tanks against vertical ground accelerations, Smart Materials and Structures 29 (5) (2020) 055017.
[13] L. Xiao, F. Sun, O. S. Bursi, Vibration attenuation and amplification of one-dimensional uncoupled and coupled systems with optimal metafoundations, Journal of Engineering Mechanics 146 (7) (2020) 04020058.
[14] Y. Achaoui, B. Ungureanu, S. Enoch, S. Brûlé, S. Guenneau, Seismic waves damping with arrays of inertial resonators, Extreme Mechanics Letters 8 (2016) 30–37.
[15] S. Krödel, N. Thomé, C. Daraio, Wide band-gap seismic metastructures, Extreme Mechanics Letters 4 (2015) 111 – 117.
[16] A. Palermo, S. Krödel, A. Marzani, C. Daraio, Engineered metabarrier as shield from seismic surface waves, Scientific reports 6 (1) (2016) 1–10.
[17] D. Colquitt, A. Colombi, R. Craster, P. Roux, S. Guenneau, Seismic metasurfaces: Sub-wavelength resonators and rayleigh wave interaction, Journal of the Mechanics and Physics of Solids 99 (2017) 379–393.
[18] E. A. Garova, A. A. Maradudin, A. P. Mayer, Interaction of rayleigh waves with randomly distributed oscillators on the surface, Phys. Rev. B 59 (1999) 13291–13296.
[19] N. Boechler, J. Eliason, A. Kumar, A. Maznev, K. Nelson, N. Fang, Interaction of a contact resonance of microspheres with surface acoustic waves, Physical Review Letters 111 (3) (2013) 036103.
[20] A. Colombi, P. Roux, S. Guenneau, P. Gueguen, R. V. Craster, Forests as a natural seismic metamaterial: Rayleigh wave bandgaps induced by local resonances, Scientific Reports 6 (1) (2016) 1–7.
[21] A. Maurel, J.-J. Marigo, K. Pham, S. Guenneau, Conversion of love waves in a forest of trees, Physical Review B 98 (13) (2018) 134311.
[22] M. Miniaci, A. Krushynska, F. Bosia, N. M. Pugno, Large scale mechanical metamaterials as seismic shields, New Journal of Physics 18 (8) (2016) 083041.
[23] A. Colombi, D. Colquitt, P. Roux, S. Guenneau, R. V. Craster, A seismic metamaterial: The resonant metawedge, Scientific Reports 6 (1) (2016) 1–6.
[24] M. A. Biot, Theory of propagation of elastic waves in a fluid-saturated porous solid. I. low-frequency range, The Journal of the Acoustical Society of America 28 (2) (1956) 168–178.
[25] G. Degrande, G. De Roeck, P. Van den Broeck, D. Smeulders, Wave propagation in layered dry, saturated and unsaturated poroelastic media, International Journal of Solids and Structures 35 (34-35) (1998) 4753–4778.
[26] J. Yang, Importance of flow condition on seismic waves at a saturated porous solid boundary, Journal of Sound and Vibration 221 (3) (1999) 391–413.
[27] A. Philippacopoulos, Waves in a partially saturated layered half-space: Analytic formulation, Bulletin of the Seismological Society of America 77 (5) (1987) 1838–1853.
[28] M. A. Biot, Mechanics of deformation and acoustic propagation in porous media, Journal of Applied Physics 33 (4) (1962) 1482–1498.
[29] M. A. Biot, Generalized theory of acoustic propagation in porous dissipative media, The Journal of the Acoustical Society of America 34 (9A) (1962) 1254–1264.
[30] A. Maznev, V. Gusev, Waveguiding by a locally resonant metasurface, Physical Review B 92 (11) (2015) 115422.
[31] J. Yang, Rayleigh surface waves in an idealised partially saturated soil, Geotechnique 55 (5) (2005) 409–414.
[32] D. Kincaid, D. R. Kincaid, E. W. Cheney, Numerical analysis: mathematics of scientific computing, Vol. 2, American Mathematical Society, 2009.
[33] P. Zheng, B. Ding, Potential method for 3d wave propagation in a poroelastic medium and its applications to lamb's problem for a poroelastic half-space, International Journal of Geomechanics 16 (2) (2016) 04015048.
[34] A. Palermo, M. Vitali, A. Marzani, Metabarriers with multi-mass locally resonating units for broad band rayleigh waves attenuation, Soil Dynamics and Earthquake Engineering 113 (2018) 265–277.
[35] X. Pu, Z. Shi, Broadband surface wave attenuation in periodic trench barriers, Journal of Sound and Vibration 468 (2020) 115130.
[36] Z. Shi, Y. Wen, Q. Meng, Propagation attenuation of plane waves in saturated soil by pile barriers, International Journal of Geomechanics 17 (9) (2017) 04017053.
[37] A. Palermo, S. Krödel, K. H. Matlack, R. Zaccherini, V. K. Dertimanis, E. N. Chatzi, A. Marzani, C. Daraio, Hybridization of guided surface acoustic modes in unconsolidated granular media by a resonant metasurface, Physical Review Applied 9 (5) (2018) 054026.
[38] R. Zaccherini, A. Colombi, A. Palermo, V. K. Dertimanis, A. Marzani, H. R. Thomsen, B. Stojadinovic, E. N. Chatzi, Locally resonant metasurfaces for shear waves in granular media, Phys. Rev. Applied 13 (2020) 034055.
[39] D. Mu, H. Shu, L. Zhao, S. An, A review of research on seismic metamaterials, Advanced Engineering Materials (2019) 1901148.
[40] C. Boutin, L. Schwan, M. S. Dietz, Elastodynamic metasurface: Depolarization of mechanical waves and time effects, Journal of Applied Physics 117 (6) (2015) 064902.
[41] M. Lott, P. Roux, S. Garambois, P. Guéguen, A. Colombi, Evidence of metamaterial physics at the geophysics scale: the metaforet experiment, Geophysical Journal International 220 (2) (2020) 1330–1339.
[42] M. Kham, J.-F. Semblat, P.-Y. Bard, P. Dangla, Seismic site–city interaction: main governing phenomena through simplified numerical models, Bulletin of the Seismological Society of America 96 (5) (2006) 1934–1951.
[43] S. Kanaun, V. Levin, M. Markov, Scattering of plane monochromatic waves from a heterogeneous inclusion of arbitrary shape in a poroelastic medium: An efficient numerical solution, Wave Motion 92 (2020) 102411.